Journal of Colloid and Interface Science 578 (2020) 471–483

Contents lists available at ScienceDirect

Journal of Colloid and Interface Science

journal homepage: www.elsevier.com/locate/jcis

Rayleigh and Rayleigh-Debye-Gans light scattering intensities and spetroturbidimetry of dispersions of unilamellar vesicles and multilamellar liposomes

An-Hsuan Hsieh, David S. Corti, Elias I. Franses *

Davidson School of Chemical Engineering, Purdue University, West Lafayette, IN 47907-2100, USA

GRAPHICAL ABSTRACT

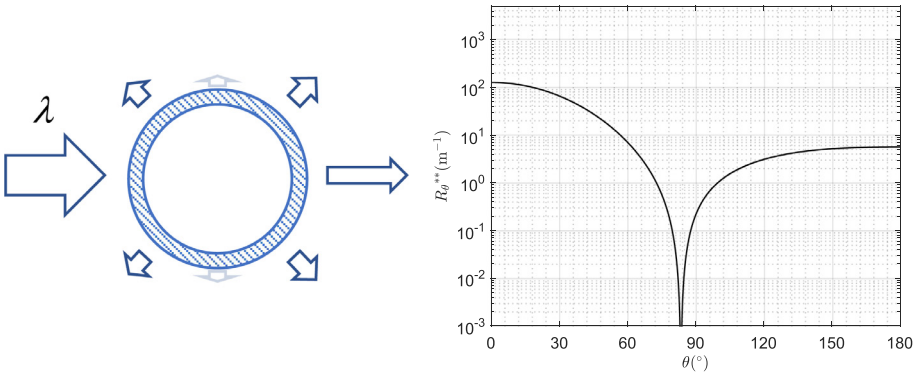

ARTICLE INFO

Article history:
Received 25 February 2020
Revised 20 May 2020
Accepted 21 May 2020
Available online 30 May 2020

Keywords:
Light scattering vesicles
Light scattering liposomes
Rayleigh scattering
Rayleigh-Debye-Gans scattering
Turbidity vesicles
Turbidity liposomes
Spectroturbidimetry vesicles
Didodecyldimethylammonium bromide vesicles
Turbidity size dependence

ABSTRACT

Hypothesis: Since the volume fraction of the surfactant bilayer(s), of thickness d_b, in a vesicle and liposome is smaller than one, the dependences of the Rayleigh (R) scattering intensity and turbidity on the particle radius a are weaker than those for a homogeneous sphere, which are proportional to a^3. The dependences of the Rayleigh-Debye-Gans (RDG) scattering intensity and turbidity on a are also weaker. Work done: The dependences of the effective relative refractive index on a, d_b, and d_w (water layer thickness) were derived. The specific Rayleigh ratio R_θ^{**} and the specific turbidity τ^{**} for single and independent scattering were derived analytically for R and RDG scattering. Spectroturbidimetry data at 25°C for a cationic double-chain surfactant, didodecyldimethylammonium bromide (DDAB) were compared to the turbidity predictions. Findings: For R scattering, R_θ^{**} and τ^{**} are proportional to $a^2 d_b$ for vesicles, and to $a^3\left(\frac{d_b}{d_w+d_b}\right)$ for liposomes. For RDG and particle radii 20–1000 nm, τ^{**} is proportional to a^n, where n is 2 to 0.4 for vesicles and 2 to 1.1 for liposomes. Turbidity data for DDAB vesicles are consistent with the RDG predictions, which are also used to estimate the vesicles' sizes. RDG applies to liposomes < 800 nm and to much larger sizes for vesicles.

1. Introduction

Aqueous dispersions of vesicles and liposomes are important in many applications, such as drug delivery [1,2], potent

* Corresponding author.
E-mail addresses: hsieh25@purdue.edu (A.-H. Hsieh), dscorti@purdue.edu (D.S. Corti), franses@purdue.edu (E.I. Franses).

https://doi.org/10.1016/j.jcis.2020.05.085
0021-9797/

Nomenclature

a	radius of a homogeneous sphere, m
a_c	radius of the central water core in a liposome, m
a_j	outer radius of the jth surfactant bilayer in a liposome, m
a_{ji}	inner radius of the jth bilayer a liposome, m
a_l	outer radius of a liposome, m
a_p	outer radius of a spherical particle, m
a_v	outer radius of a vesicle, m
a_v^*	average radii of DDAB vesicles, m
a_{vi}	inner radius of a vesicle, m
$\bar{a}_j$	average radius of the jth bilayer in a liposome, m
$\bar{a}_v$	average radius of the bilayer in a vesicle, m
A	absorbance due to scattering
$C_1(x)$	cosine integral function
d_b	bilayer thickness in a vesicle, m
d_w	thickness of each water layer in a liposome, m
$\boldsymbol{E}$	uniform electric field (in SM), V/m
f_l	form factor of a liposome
f_p	intraparticle scattering factor or form factor of a particle
f_s	form factor of a homogeneous sphere
f_{s,a_j}	form factor of a sphere of radius a_j
$f_{s,a_{ji}}$	form factor of a sphere of radius a_{ji}
f_{s,a_v}	form factor of a sphere of radius a_v
$f_{s,a_{vi}}$	form factor of a sphere of radius a_{vi}
f_v	form factor of a vesicle
$f_{v,j}$	form factor of the jth bilayer in a liposome
g_l	wavelength exponent for liposomes
g_p	wavelength exponent for particles
g_s	wavelength exponent for homogeneous spheres
g_v	wavelength exponent for vesicles
h	parameter defined in Eq. (SM.60), m^{-1}
i_s	scattered light intensity, W/m^2
$i_{s,N}$	scattered light intensity per unit volume, W/m^5
$i_{s,N}(r,\theta,z)$	scattered light intensity per unit volume at the coordinate position z, W/m^5
$i_{s,N,R}$	scattered light intensity per unit volume in the R regime, W/m^5
$i_{s,N,RDG}$	scattered light intensity per unit volume in the RDG regime, W/m^5
$i_{s,R}$	scattered light intensity in the R regime, W/m^2
$i_{s,RDG}$	scattered light intensity in the RDG regime, W/m^2
I_0	unpolarized incident light intensity, W/m^2
I_t	transmitted light intensity, W/m^2
$I(z)$	incident light intensity at the coordinate position z, W/m^2
j	number of surfactant bilayers in a liposome
$j_1(x)$	first order spherical Bessel function
K	total number of surfactant bilayers in a liposome
ℓ	beam pathlength, m
m_l	effective relative refractive index of a liposome
m_p	effective relative refractive index of a particle
m_s	relative refractive index of a homogeneous sphere or a surfactant bilayer
m_v	effective relative refractive index of a vesicle
M_l	term of effective relative refractive index of a liposome (in SM)
M_s	term of effective relative refractive index of a homogeneous sphere
M_v	term of effective relative refractive index of a vesicle
n_m	refractive index of the medium
n_p	effective refractive index of a particle
n_s	refractive index of a homogeneous sphere or a surfactant bilayer
N_l	number density of liposomes (in SM), m^{-3}
N_p	number density of particles, m^{-3}
N_s	number density of homogeneous spheres (in SM), m^{-3}
N_v	number density of vesicles (in SM), m^{-3}
$\boldsymbol{p}$	electric dipole moment (in SM), C·m
$P_{s,N}(z)$	loss of power from the incident light per unit length at the coordinate position z, W/m^3
q	magnitude of the scattering vector, m^{-1}, Eq. (22)
Q_l	dissipation factor of a liposome
Q_p	dissipation factor of a particle
Q_s	dissipation factor of a sphere
Q_v	dissipation factor of a vesicle
r	distance of observation or a radius of a closed surface of a sphere, m
R_θ	Rayleigh ratio, m^{-1}
R_θ^{**}	specific Rayleigh ratio, m^{-1}
V_l	volume of an entire liposome (in SM), m^3
$V_{l,b}$	volume of the surfactant bilayers in a liposome (in SM), m^3
V_s	volume of a homogeneous sphere (in SM), m^3
V_v	volume of an entire vesicle, m^3
$V_{v,b}$	volume of the surfactant bilayers in a vesicle, m^3
$V_{v,j}$	volume of the jth bilayer, m^3
w_{DDAB}	DDAB weight fraction
w_{surf}	total surfactant weight fraction
x_s	dimensionless size (see Eq. (SM.68))
$\bar{x}_v$	dimensionless size (see Eq. (SM.78)
$X_{pm,R}$	dimensionless quantity defined in Eq. (1)
$X_{pp,R}$	dimensionless quantity defined in Eq. (1)
$X_{p,RDG}$	dimensionless quantity defined in Eq. (4)
$X_{v,RDG}$	dimensionless quantity defined in Eq. (SM.41)
z	coordinate position, m
α_l	excess polarizability of a liposome (in SM), m^3
α_s	excess polarizability of a homogeneous sphere (in SM), m^3
α_v	excess polarizability of a vesicle (in SM), m^3
$\widehat{\alpha}_l$	effective specific polarizability of a liposome (in SM)
$\widehat{\alpha}_s$	specific bilayer polarizability or effective specific polarizability of a homogeneous sphere
$\widehat{\alpha}_v$	effective specific polarizability of a vesicle
β	a collective term, see Eq. (18), m^{-4}
γ	a collective term defined indirectly in Eq. (5), W/m^8
γ_E	Euler gamma constant
ϵ_m	permittivity of the medium (in SM), C/Vm
θ	scattering angle
λ_0	wavelength of light in vacuum, m
ρ_{disp}	mass density of the dispersion, kg/m^3
ρ_{surf}	mass density of the surfactant bilayer, kg/m^3
τ	turbidity
τ_R	turbidity in the R regime (in SM)
τ_{RDG}	turbidity in the RDG regime (in SM)
τ^*	turbidity per unit pathlength (in SM), m^{-1}
τ^{**}	specific turbidity, m^{-1}
τ^{**}_R	specific turbidity in the R regime, m^{-1}
τ^{**}_{RDG}	specific turbidity in the RDG regime, m^{-1}
ϕ	azimuthal angle
ϕ_l	volume fraction of liposomes in a dispersion (in SM)
$\phi_{l,b}$	volume fraction of the surfactant bilayers in a liposome
$\phi_{p,b}$	volume fraction of the surfactant bilayer in a vesicle or bilayers in a liposome
ϕ_{surf}	surfactant volume fraction for the dispersion
ϕ_v	volume fraction of vesicles in a dispersion (in SM)
$\phi_{v,b}$	volume fraction of the surfactant bilayer in a vesicle
DLS	dynamic light scattering
R	Rayleigh

RDG	Rayleigh-Debye-Gans	ST	spectroturbidimetry
SLS	static light scattering	TEM	transmission electron microscopy

immunosuppressants [3], compartments or templates for synthesis [4,5], and model systems for biological membranes [6,7]. The formation of liposomes and vesicles, usually formed by double-chain surfactants, depends on the phase behavior of the surfactant-water system, and the methods of their preparation. Normally, when the surfactant is dispersed by stirring, initially it forms liposomes (multilamellar particles, or "onions"). Upon further stirring, or sonication, or extrusion through a microporous membrane, it can form vesicles (unilamellar particles) [1,8].

To better understand the phase and dispersion behavior of dispersions of vesicles and liposomes, it is important to confirm their morphologies and shapes and to determine their size distributions. The most direct method for determining their shapes is via cryo-TEM (transmission electron microscopy), allowing visualization of vesicles and liposomes. Cryo-TEM can yield information about particle size distributions, but it is difficult to use and costly [9,10]. In addition, because the thickness of the specimens observable by cryo-TEM with minimal multiple scattering of electrons is less than 1 μm, liposomes and vesicles larger than ca. 0.5 μm are excluded during the sample preparation [11,12].

The dynamic light scattering (DLS) method, in which the autocorrelation function of the fluctuating scattered light intensities is measured at a specific angle and wavelength, is often used for determining the hydrodynamic radii of particles, from ca. 5 to 2000 nm (2 μ m), and the particle size distributions, or their polydispersity [[13], pp. 236–242; [14]]. The static light scattering (SLS) method, in which the time-averaged scattered light intensities, $i_{s,N}$ by a dispersion of particles are measured at various angles and wavelengths, can also be used for determining the radii of spherical particles, their molecular masses, and sometimes their radii of gyration, which are a measure of the particles shape [[13], pp. 215–223; [15]]. Moreover, the turbidity τ, or absorbance A, due to scattering by suspended particles can also be used for determining the particle size/shape information, either from its absolute value or from its wavelength dependence. This spectroturbidimetry technique (ST), is relatively easy to use, and can be done with a common spectrophotometer [16–20]. Therefore, it is important to determine what information can be obtained from the SLS and ST methods. This has been done previously to a limited extent [17,21–23]. Nonetheless, the general problems of how $i_{s,N}$ and τ for single and independent scattering vary with the vesicle or liposome radius for the two simplest light scattering regimes, the Rayleigh regime (R) and the Rayleigh-Debye-Gans regime (RDG), have not been fully addressed. Here, new analytical solutions for these problems for vesicles and liposomes are derived. We show the complete solutions of the "direct problem," of calculating the R and RDG intensities and turbidities for single and independent scattering (usually valid for dilute dispersions) for vesicles and liposomes of a fixed size (a monodisperse size distribution) [[24], pp. 9-11]. No general equations for any size or refractive index, analogous to the Mie theory for spheres, are available [25]. The Mie-type problem would be quite difficult to solve, and probably too complicated to be cast in analytical form, although some general numerical solutions have been reported recently [20]. In our analysis, we use published expressions of the RDG form factors of homogeneous spheres, vesicles, and liposomes, and combine them with the R expressions to derive the equations of the specific Rayleigh ratios, specific turbidities, and turbidity wavelength exponents for wavelength-dependent refractive indices. These equations can be used for estimating the particle sizes from SLS and ST methods. These results are applicable to a broad range of vesicle sizes.

Rayleigh (R) scattering is the simplest scattering regime. It is valid when the external electromagnetic field in the medium appears to be uniform in the scale of the particle size [[26], p. 75; [25], pp. 84–88; [24], p. 140], or when the electromagnetic field appears to be uniform inside the particle, or when

$$X_{pm,R} \equiv \frac{4\pi n_m a_p}{\lambda_0} \ll 1 \quad \text{or} \quad X_{pp,R} \equiv \frac{4\pi n_p a_p}{\lambda_0} \ll 1 \tag{1}$$

where n_m is the medium's refractive index, a_p is the outer radius of the spherical particle, or other characteristic length for other shapes, λ_0 is the wavelength of light in vacuum, and n_p is the effective refractive index of the particle. For particles for which $n_p \geqslant n_m$, or when the relative refractive index of the particle, $m_p \equiv n_p/n_m \geqslant 1$ [[24], p. 100; [25], p. 35]. In Eq. (1), the latter implies the former. In practice, when estimating the maximum size for the validity of R scattering, one can use the following equation [[25], pp. 84–88]

$$X_{pp,R} = \frac{4\pi n_p a_p}{\lambda_0} = 0.1 \text{ or } 0.2 \tag{2}$$

For homogeneous spheres in water with a typical value of n_p = 1.466 for a surfactant, and for λ_0 = 350 to 700 nm, the maximum values of a_p range from 2 to 4 nm (for the 0.1 limit) or 4 to 8 nm (for the 0.2 limit). The corresponding range for vesicles of DDAB is slightly larger, due to a smaller effective values of n_p: from 2 to 5 nm, and from 4 to 10 nm.

However, the sizes of most practical vesicles and liposomes fall outside the R regime, and they may fall in the RDG regime. The conditions for the validity of the equations of the RDG scattering regime are [[26], p. 85; [25], p.415]; [24], p. 159]

$$| m_p - 1 | \ll 1 \quad \text{or} \quad | m_p - 1 | = 0.1 \text{ or } 0.2 \tag{3}$$

and

$$X_{p,RDG} \equiv \frac{4\pi n_m a_p}{\lambda_0} | m_p - 1 | \ll 1 \quad \text{or} \quad X_{p,RDG} = \frac{4\pi n_m a_p}{\lambda_0} \\ | m_p - 1 | = 0.1 \text{ or } 0.2 \tag{4}$$

Eq. (3) implies that the incident wave remains essentially unchanged at the interface between the particle and the medium, and is generally valid for most surfactants in water for which $m_p \cong$ 1.05 to 1.15. For Eq. (4), the electric field within the particle changes little in phase or amplitude from that in the surrounding medium. For homogeneous spheres with m_p = 1.10, and for λ_0 = 350 to 700 nm, the a_p-range for RDG scattering is from 20 to 40 nm (for the 0.1 limit) or 40 to 80 nm (for the 0.2 limit). As discussed later, the allowable sizes are, however, much larger for vesicles (>1000 nm) and liposomes (ca. 800 nm) because the effective values of m_p for these inhomogeneous particles are much smaller (see Section 3). The key idea is that the effective average refractive indices for vesicles and liposomes depend on the volume fraction of the surfactant bilayer in the particles, and hence on their sizes and on the values of d_b and d_w. For vesicles, being comprised of a single surfactant bilayer, m_p approaches the value of 1.0 as the vesicle radius increases. For very large vesicles, therefore, the RDG conditions are also satisfied, a result which has been

previously unnoticed. Hence, various dispersions of interest that are comprised of vesicles or liposomes can be analyzed using the results obtained for the RDG regime.

The article outline is as follows. Section 2 covers the theory of R scattering for vesicles and liposomes. By focusing on the effective average refractive indices of vesicles, we find a surprising dependence of the scattered intensity, the specific Rayleigh ratio, and the specific turbidity on the square of the vesicle radius, rather than on the cube of the radius as for homogeneous spheres or for liposomes. Section 3 covers the theory of RDG scattering, where an expression for the absolute scattered intensity, or specific Rayleigh ratio, of vesicles and liposomes is provided for the first time. Previous reports were focused on the form factor, and hence considered only the relative scattered intensities at various angles. Several general and specific sample calculations for vesicles and liposomes of an example of a specific surfactant, DDAB (didodecyldimethylammonium bromide), in water, are presented in Section 4. DDAB vesicles have been found to improve the stability of suspensions of dense particles against sedimentation [27,28]. The properties and applications of DDAB liposomes and vesicles have been studied extensively [12,27–33]. Reliable estimates have been determined for the vesicle and liposome bilayer thickness d_b and the water layer thickness d_w in liposomes. The analysis and sample calculations provided here aim at generating insights on the direct problem, which may affect later the addressing of the solution of the "inverse" problem, of determining average particle sizes and their size distributions from measured scattered intensities or turbidities [[24], pp. 9–11]. Some data of turbidities of DDAB vesicles are shown in Section 5, and are used along with the RDG equations to estimate average vesicle sizes. These sizes are compared to the sizes obtained from DLS data. Finally, the main conclusions are presented in Section 6.

2. Theory of Rayleigh scattering for spherical particles

2.1. Scattered light intensities

2.1.1. Scattering for one particle

For a homogeneous sphere of radius a, comprised of scattering elements with a relative refractive index m_s, a wavelength of light in vacuum λ_0 with an unpolarized incident light intensity I_0 (in W/m^2), and surrounded by a medium with a refractive index n_m, the scattered light intensity i_s (in W/m^2) above that of the background medium, at a distance r and a scattering angle θ, is for the R regime as follows [[24], p. 132],

$$i_s = \frac{8\pi^4 a^6}{r^2}\left(\frac{n_m}{\lambda_0}\right)^4 {M_s}^2(1+\cos^2\theta)I_0 = \gamma a^6 \tag{5}$$

and the term γ is the product of all the terms in Eq. (5) except a^6 and where M_s is defined as

$$M_s \equiv \frac{{m_s}^2-1}{{m_s}^2+2} \tag{6}$$

If the incident light is vertically or horizontally polarized, the term $(1+\cos^2\theta)$ in Eq. (5) is replaced by the term 2 or $2\cos^2\theta$, respectively.

For an equation analogous to Eq. (5) for a vesicle or a liposome, one must account for scattering elements which are no longer distributed uniformly throughout the particle. The effective average relative refractive indices m_v and m_l for a vesicle or a liposome are smaller than m_s, and depend on the volume fraction $\phi_{v,b}$ of the bilayer in a vesicle, or the volume fraction $\phi_{l,b}$ of all the bilayers in a liposome. For a vesicle with an outer radius a_v and a bilayer thickness d_b (see Fig. 1), the volume fraction of the bilayer $\phi_{v,b}$ in the particle is,

$$\phi_{v,b} = \frac{{a_v}^3-(a_v-d_b)^3}{{a_v}^3} = 3\left(\frac{d_b}{a_v}\right) - 3\left(\frac{d_b}{a_v}\right)^2 + \left(\frac{d_b}{a_v}\right)^3 \tag{7}$$

or approximately $3d_b/a_v$ in the limit of $a_v \gg d_b$.

Because only those elements in the bilayer scatter light, above the scattering of the background medium, the term M_s in Eq. (5) is replaced by M_v

$$M_v \equiv \frac{{m_v}^2-1}{{m_v}^2+2} = \phi_{v,b}M_s \tag{8}$$

where m_v is the effective relative refractive index of the entire vesicle (see Fig. 1). The derivation of Eq. (8) and the analogue for a liposome are shown in the Supporting Material, Section A (SM, A). From Eq. (5), and invoking Eq. (8), the R scattered light intensity for one vesicle is or, in the limit of $a_v \gg d_b$,

$$i_s = \gamma {a_v}^6 {\phi_{v,b}}^2 \approx 9\gamma {a_v}^4 {d_b}^2 \tag{9}$$

Hence, the scattered light intensity of a vesicle has a weaker dependence on the particle radius than that of a homogeneous sphere, being proportional to ${a_v}^4$ rather than to a^6.

For one liposome, the R scattered light intensity is given by a general equation in terms of the number K of bilayers in a liposome; see the equations and derivations in SM, A. For large liposomes, or when $K \gg 1$, the approximate equation is

$$i_s = \gamma {a_l}^6 {\phi_{l,b}}^2 \approx \gamma {a_l}^6 \left(\frac{d_b}{d_w+d_b}\right)^2 \tag{10}$$

Therefore, for a large liposome, i_s is proportional to ${a_l}^6$, but it is quite smaller than that of a homogeneous sphere by a factor of about $\left(\frac{d_b}{d_w+d_b}\right)^2$.

2.1.2. Dispersions of particles

For single and independent scattering from a dispersion with a particle number density N_p (number of particles per unit volume), the scattered light intensity per unit volume, in W/m^5, is given by [[25], p. 36]

$$i_{s,N} = N_p i_s \tag{11}$$

For vesicles with a total surfactant weight fraction w_{surf}, the surfactant volume fraction for the dispersion is

$$\phi_{surf} = w_{surf}\left(\frac{\rho_{disp}}{\rho_{surf}}\right) \tag{12}$$

where ρ_{disp} is the mass density of the dispersion and ρ_{surf} is the mass density of the surfactant bilayer.

In general, or when $\rho_{disp} \approx \rho_{surf}$,

$$i_{s,N} = \frac{3}{4\pi}\phi_{surf}\gamma {a_p}^3 \phi_{p,b} \approx \frac{3}{4\pi} w_{surf}\gamma {a_p}^3 \phi_{p,b} \tag{13}$$

where $\phi_{p,b}$ is the volume fraction of the surfactant bilayer in a vesicle or bilayers in a liposome. The derivation and expressions of $i_{s,N}$ of spherical particles in the R regime are shown in the Supporting Material, Section B (SM, B). Therefore, the size dependence of $i_{s,N}$ is weaker for vesicles than for homogeneous spheres or for liposomes, because the volume fraction of the surfactant bilayer in the vesicle $\phi_{v,b}$ decreases with increasing radius a_v.

Instead of using $i_{s,N}$, which depends on r and I_0, the following intrinsic parameter R_θ, called the "Rayleigh ratio," [[13], p. 206; [25], p. 38], in units of m^{-1}, is more useful, because it is independent of r and I_0.

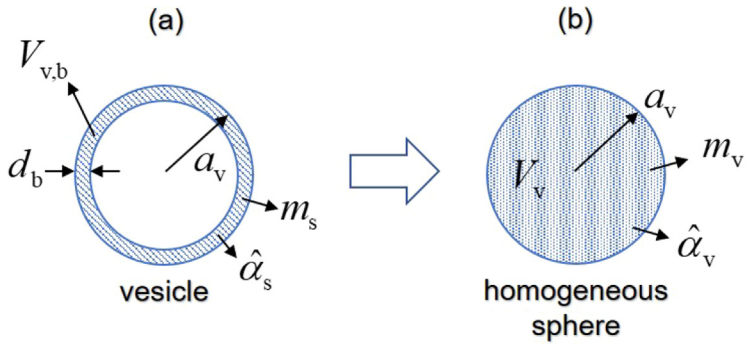

Fig. 1. (a) A vesicle of outer radius a_v, total volume V_v, bilayer thickness d_b, specific bilayer polarizability $\hat{\alpha}_s$, and relative refractive index m_s; (b) a homogeneous sphere with the same radius a_v and total volume V_v, but with a smaller effective relative refractive index $m_v < m_s$ and a smaller specific polarizability $\hat{\alpha}_v < \hat{\alpha}_s$. This homogeneous sphere yields the same combined R scattering intensities as the vesicle.

$$R_\theta \equiv \frac{i_{s,N} r^2}{6\pi^3 I_0} \tag{14}$$

The specific Rayleigh ratio, $R_\theta{}^{**}$, where

$$R_\theta{}^{**} \equiv \frac{R_\theta}{w_{surf}} \tag{15}$$

is independent of w_{surf} for single and independent scattering. Hence, it is an intrinsic property of the particle size, shape, and refractive index. The general expressions of Eqs. (14) and (15) for spherical particles are shown in the Supporting Material, Section C (SM, C).

2.2. Turbidities for dispersions of particles

For a nonabsorbing sample with an incident intensity I_0 at $z = 0$, a transmitted intensity I_t at $z = \ell$, and a pathlength ℓ, the differential energy balance for the intensity $I(z)$ is [[25], p. 38]

$$-dI(z) = P_{s,N}(z)dz \tag{16}$$

where $P_{s,N}(z)$ is the total energy per unit time of the intensity $I(z)$ that is scattered, or "lost" per unit pathlength. It is found by integrating the scattered intensity $i_{s,N}(r,\theta,z)$ over a closed surface of a sphere with intensity $I(z)$ and a radius r over an azimuthal angle ϕ (0 to 2π) and a scattering angle θ (0 to π),

$$P_{s,N}(z) \equiv \int_{\phi=0}^{2\pi} \int_{\theta=0}^{\pi} i_{s,N}(r,\theta,z) r^2 \sin\theta d\theta d\phi \tag{17}$$

For R scattering, with Eq. (13) for $i_{s,N}$,

$$P_{s,N}(z) = 32\pi^4 \left(\frac{n_m}{\lambda_0}\right)^4 I(z) {M_s}^2 \phi_{surf} {a_p}^3 \phi_{p,b} \tag{18}$$

where for convenience, we have defined the quantity $\beta \equiv 32\pi^4 (n_m/\lambda_0)^4 {M_s}^2$.

In general, for R scattering, the specific turbidity of the spherical particles is

$$\tau^{**}{}_R = \beta \left(\frac{\rho_{disp}}{\rho_{surf}}\right) {a_p}^3 \phi_{p,b} \tag{19}$$

The definition of the turbidity and the specific turbidity and the corresponding expressions of spherical particles are shown in the Supporting Material, Section D (SM, D).

3. Theory of Rayleigh-Debye-Gans (RDG) scattering for spherical particles

3.1. Size limits for spherical particles for applicability of the RDG equations

If the particle size exceeds the limit of applicability of the R scattering, and if m_s is small enough, e.g. $m_s < 1.2$, the RDG scattering regime may be potentially applicable. To determine the practical RDG regime size limit for vesicles and liposomes, we consider one specific set of examples for water, in which a constant value of $n_m = 1.333$ is used, and for a surfactant with $m_s = 1.10$ (for homogeneous spheres), which is typical for surfactants and the surfactant DDAB, which is used here. For $\lambda_0 = 700$ nm, the calculated values of the quantity $X_{p,RDG}$ in Eq. (4) for homogeneous spheres, or for vesicles with $d_b = 2.4$ nm, or for liposomes with $d_b = 2.4$ nm and $a_c = d_w = 50$ nm (see Fig.SM1), are shown in Fig. 2. For homogeneous spheres, and $X_{p,RDG} = 0.1$ or 0.2, the size limits for a are 42 or 84 nm. For liposomes, these limits are ca. 800 or 2000 nm. No such limits were found for vesicles since m_v approaches 1 fast enough as the vesicle size increases and then $X_{p,RDG} < 0.1$. (See SM, E for a derivation of the limit value of $X_{p,RDG}$ for large vesicles.).

3.2. RDG Scattered light intensities

3.2.1. RDG scattering for one particle

The total scattered intensity in the RDG regime is equal to the R scattered intensity (Eqs. (5), (9), or (10)) multiplied by the square of the intraparticle scattering factor or form factor, f_p [[25], pp. 414–417],

$$i_{s,RDG} = i_{s,R} {f_p}^2 \tag{20}$$

For a homogeneous sphere of radius a, the form factor was first derived by Rayleigh [[25], pp. 414–417], and is given by

$$f_s = \frac{3}{q^3 a^3}[\sin(qa) - qa\cos(qa)] = 3\frac{j_1(qa)}{qa} \tag{21}$$

where q is the magnitude of the scattering vector [23],

$$q \equiv \frac{4\pi n_m}{\lambda_0} \sin\left(\frac{\theta}{2}\right) \tag{22}$$

and $j_1(x) = \sin(x)/x^2 - \cos(x)/x$ is the first order spherical Bessel function [23]. The scattered intensity depends strongly on θ and can be zero when the form factor is zero (see Eq. (21)) [[24] p. 163]. The first several roots (zero intensity) of Eq. (21) are shown in SM, F. The first root occurs at $qa = 4.4934$. With $n_m = 1.333$

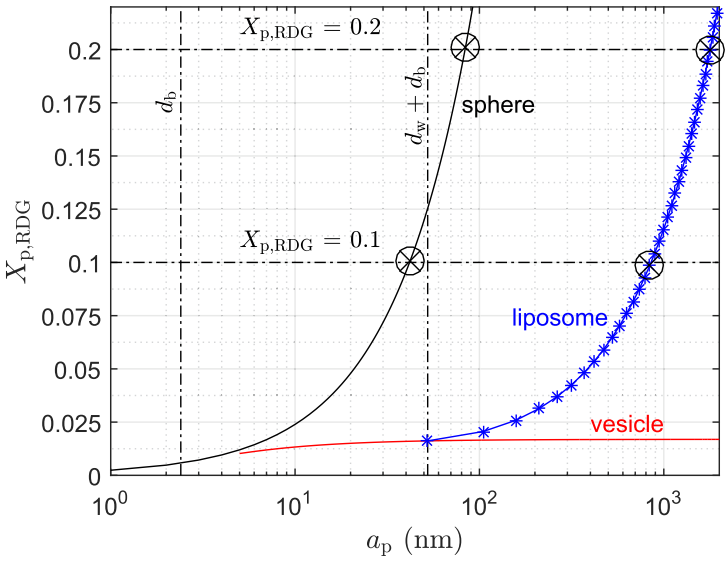

Fig. 2. Values of $X_{p,RDG}$ of the RDG validity condition (Eq. (4)) vs. particle size for homogeneous spheres, vesicles, and liposomes, for $m_s = 1.10$ and $\lambda_0 = 700$ nm, and for $d_b = 2.4$ nm and $a_c = d_w = 50$ nm. The RDG size limits for spheres and liposomes for $X_{p,RDG} = 0.1$ or 0.2 are shown as circles. No limits are found for vesicles.

and $\lambda_0 = 350$ nm, $qa < 4.4934$ when $a < 94$ nm. Hence, for $a < 94$ nm, $i_{s,RDG} > 0$ at all angles.

The form factor for a vesicle is [34]

$$f_v = \frac{3a_v{}^3 \frac{j_1(qa_v)}{qa_v} - 3a_{vi}{}^3 \frac{j_1(qa_{vi})}{qa_{vi}}}{a_v{}^3 - a_{vi}{}^3} = \frac{a_v{}^3 f_{s,a_v} - a_{vi}{}^3 f_{s,a_{vi}}}{a_v{}^3 - a_{vi}{}^3} \tag{23}$$

where $a_{vi} = a_v - d_b$ is the inner radius of a vesicle, f_{s,a_v} is the form factor of a sphere of radius a_v, and $f_{s,a_{vi}}$ is the form factor of a sphere of radius a_{vi}. As the value of a_{vi} approaches 0 (for which a vesicle becomes a homogeneous sphere), Eq. (23) approaches Eq. (21). A much simpler approximate form of Eq. (23) for a small bilayer thickness (or a thin spherical shell) is [22]

$$f_v \approx \frac{\sin(q\bar{a}_v)}{q\bar{a}_v} \tag{24}$$

in which $\bar{a}_v = (a_v + a_{vi})/2$, the average radius of the bilayer in a vesicle. Comparisons of the predictions of Eqs. (23) and (24), shown in SM, G, indicate that Eq. (24) is a very good approximation of Eq. (23) for most typical vesicle sizes.

The form factor of a liposome f_l is [34],

$$f_l = \frac{\sum_{j=1}^{K} V_{v,j} f_{v,j}}{\sum_{j=1}^{K} V_{v,j}} \tag{25}$$

where $f_{v,j}$ is the form factor of the jth bilayer in a liposome (given by Eq. (23)) and $V_{v,j}$ is the volume of the jth bilayer. Each bilayer in a liposome is treated as an independent vesicle weighted by its volume. Combining Eqs. (23) and (25) results in the equation

$$f_l = \frac{\sum_{j=1}^{K} \left(a_j{}^3 f_{s,a_j} - a_{ji}{}^3 f_{s,a_{ji}} \right)}{\sum_{j=1}^{K} \left(a_j{}^3 - a_{ji}{}^3 \right)} \tag{26}$$

where $a_{ji} = a_j - d_b$ is the inner radius of the jth bilayer in a liposome, f_{s,a_j} is the form factor of a sphere of radius a_j, and $f_{s,a_{ji}}$ is the form factor of a sphere of radius a_{ji}. A simpler approximate form of Eq. (26) is obtained for the limit of small bilayer thicknesses as in Eq. (24).

$$f_l \approx \frac{\sum_{j=1}^{K} j^2 \frac{\sin(q\bar{a}_j)}{q\bar{a}_j}}{\sum_{j=1}^{K} j^2} = \frac{6 \sum_{j=1}^{K} j^2 \frac{\sin(q\bar{a}_j)}{q\bar{a}_j}}{K(K+1)(2K+1)} \tag{27}$$

where the average radius of the jth bilayer is $\bar{a}_j = a_j - \frac{d_b}{2}$. For large liposomes ($K \gg 1$), Eq. (27) reduces to

$$f_l \approx \frac{3}{K^3} \sum_{j=1}^{K} j^2 \frac{\sin(q\bar{a}_j)}{q\bar{a}_j} \tag{28}$$

Further details of the derivations of Eqs. (27) and (28) are given in SM, H.

3.2.2. RDG scattered intensities for dispersions of particles

The general equation for $i_{s,N,RDG}$ for the RDG regime is given by the product of $i_{s,N,R}$ for the R regime and the square of the form factor,

$$i_{s,N,RDG} = i_{s,N,R} f_p{}^2 \tag{29}$$

Hence, using Eqs. (13) and (29), for RDG scattering

$$i_{s,N} = \frac{3}{4\pi} \phi_{surf} \gamma a_p{}^3 \phi_{p,b} f_p{}^2 \tag{30}$$

Then, in general, using Eqs. (5), (14), (15), and (30), the specific Rayleigh ratio for spherical particles is

$$R_\theta{}^{**} = a_p{}^3 \left(\frac{n_m}{\lambda_0} \right)^4 M_s{}^2 (1 + \cos^2\theta) \phi_{p,b} \left(\frac{\rho_{disp}}{\rho_{surf}} \right) f_p{}^2 \tag{31}$$

The expressions of the specific Rayleigh ratio of spherical particles in the RDG regime are shown in SM, C.

3.3. RDG turbidities for dispersions of particles

The specific turbidity for the dispersion in the RDG regime, in general, is the product of the specific R turbidity (Eq. 19) and the dissipation factor Q_p

$$\tau^{**}{}_{RDG} = \beta\left(\frac{\rho_{disp}}{\rho_{surf}}\right) a_p{}^3 \phi_{p,b} Q_p \tag{32}$$

where Q_p now is the integral of the square of the form factor [21],

$$Q_p \equiv \frac{3}{8}\int_0^\pi f_p{}^2 (1+\cos^2\theta)\sin\theta d\theta \tag{33}$$

The derivation and expressions of the RDG turbidity for spherical particles are shown in SM, D.

For homogeneous spheres, or when $\rho_{disp} \approx \rho_{surf}$,

$$\tau^{**}{}_{RDG} = \tau^{**}{}_R Q_s \approx \beta a^3 Q_s \tag{34}$$

Q_s is evaluated by substituting f_s from Eq. (21) to Eq. (33) [[25], pp. 417–418]. A change of variable from θ to q allows for Q_s to be determined analytically using integral tables [35,36]. Equivalently, a commercial software package of computer algebra systems, Wolfram Mathematica is used. The result is (see SM, I)

$$Q_s = \frac{27}{x_s{}^6}\left\{\frac{x_s{}^4}{4} + \frac{5x_s{}^2}{4} + (1-x_s{}^2)[\gamma_E - C_I(2x_s) + \ln(2x_s)] + \frac{7}{8}\cos(2x_s) - \frac{x_s}{4}\sin(2x_s) - \frac{7}{8}\right\} \tag{35}$$

where $x_s \equiv 4\pi n_m a/\lambda_0$, γ_E is the Euler gamma constant, and

$$C_I(x) = -\int_x^\infty \frac{\cos t}{t} dt \tag{36}$$

is the cosine integral function. Even though Eq. (33) can be integrated numerically, having an analytical Eq. (35) facilitates the calculation of $\tau^{**}{}_{RDG}$ and related parameters. Moreover, it is quite beneficial for calculating analytically the wavelength exponent g_p (Section 3.4) and for later solving the general inverse problem.

For vesicles, we find similarly

$$\tau^{**}{}_{RDG} \approx \beta a_v{}^3 \phi_{v,b} Q_v \approx 3\beta a_v{}^2 d_b Q_v \tag{37}$$

When Eq. (33) is evaluated by using the approximate f_v (Eq. (24)), a new analytical expression for Q_v is derived (see SM, I),

$$Q_v \approx \frac{3}{\bar{x}_v{}^6}\left\{-\frac{\bar{x}_v{}^4}{4} - \frac{\bar{x}_v{}^2}{4} + \frac{\bar{x}_v{}^4}{2}\left[\gamma_E - C_I\left(2\bar{x}_v\right) + \ln\left(2\bar{x}_v\right)\right] + \frac{3-4\bar{x}_v{}^2}{8}\cos\left(2\bar{x}_v\right) + \frac{3\bar{x}_v}{4}\sin\left(2\bar{x}_v\right) - \frac{3}{8}\right\} \tag{38}$$

where $\bar{x}_v \equiv 4\pi n_m \bar{a}_v/\lambda_0$. A more complex formula can be obtained for the exact vesicle form factor of Eq. (23), but is not shown here.

For liposomes, we find

$$\tau^{**}{}_{RDG} \approx \beta a_l{}^3 \phi_{l,b} Q_l \approx \beta a_l{}^3 \left(\frac{d_b}{d_w + d_b}\right) Q_l \tag{39}$$

An analytical expression for Q_l, with either the approximate or the exact form factor can be generated, but is beyond the scope of this article.

3.4. Wavelength dependence of turbidities

The wavelength exponent g_p, which is the measure of the dependence of the specific turbidity τ^{**} on the wavelength, is defined as [21]

$$g_p \equiv -\frac{\partial \log \tau^{**}}{\partial \log \lambda_0} \tag{40}$$

In the R regime, when the dependence of n_m and n_p on λ_0 is not considered, since the only dependence of τ^{**} on wavelength is in the term $1/\lambda_0{}^4$, the value of g_p is 4, independent of the wavelength. In the RDG regime, if the dependence of n_m and n_p (and hence m_p) on λ_0 is also ignored, then g_p is smaller than 4 and depends on λ_0,

$$g_p = -\lambda_0\left(\frac{\partial \ln \beta}{\partial \lambda_0} + \frac{\partial \ln Q_p}{\partial \lambda_0}\right) = 4 - \frac{\lambda_0}{Q_p}\frac{\partial Q_p}{\partial \lambda_0} \tag{41}$$

By differentiation of Q_p in Eq. (35), for homogeneous spheres, we obtain

$$g_s = -2 + \left\{\frac{8x_s{}^4 + 12x_s{}^2 - 16x_s{}^2[\gamma_E - C_I(2x_s) + \ln(2x_s)] + (4x_s{}^2 - 8)\cos(2x_s) - 16x_s\sin(2x_s) + 8}{2x_s{}^4 + 10x_s{}^2 - 7 + 8(1-x_s{}^2)[\gamma_E - C_I(2x_s) + \ln(2x_s)] + 7\cos(2x_s) - 2x_s\sin(2x_s) - 7}\right\} \tag{42}$$

As x_s in the numerator and the denominator approaches 0, g_s approaches the R limit of 4, as expected. For very large values of x_s, when the $x_s{}^4$ terms in the numerator and the denominator in Eq. (42) are dominant, g_s approaches the value of $-2 + 8/2 = 2$.

For vesicles, from Eqs. (38) and (41), we obtain similarly,

$$g_v \approx -2 + \left\{\frac{-4\bar{x}_v{}^4 - 4\bar{x}_v{}^2 + 16\bar{x}_v{}^4\left[\gamma_E - C_I\left(2\bar{x}_v\right) + \ln\left(2\bar{x}_v\right)\right] + 4\left(\bar{x}_v{}^2 - \bar{x}_v{}^4\right)\cos\left(2\bar{x}_v\right) + 8\bar{x}_v{}^3\sin\left(2\bar{x}_v\right)}{-2\bar{x}_v{}^4 - 2\bar{x}_v{}^2 + 4\bar{x}_v{}^4\left[\gamma_E - C_I\left(2\bar{x}_v\right) + \ln\left(2\bar{x}_v\right)\right] + \left(3 - 4\bar{x}_v{}^2\right)\cos\left(2\bar{x}_v\right) + 6\bar{x}_v\sin\left(2\bar{x}_v\right) - 3}\right\} \tag{43}$$

For very large values of $\bar{x}_v$, when the $\bar{x}_v{}^4\ln(2\bar{x}_v)$ terms in the numerator and the denominator in Eq. (43) are dominant, g_v approaches the value of $-2 + 16/4 = 2$, as a strict lower bound of g_v.

For liposomes, with the approximate expression of the form factor for small bilayer thicknesses in Eq. (27), we obtain the following integral expression

$$g_l \approx 2 + \frac{12}{K(K+1)(2K+1)} \times \frac{\sum_{j=1}^{K} j^2 \int_0^\pi f_l \cos\left(q\bar{a}_j\right)(1+\cos^2\theta)\sin\theta d\theta}{\int_0^\pi f_l{}^2(1+\cos^2\theta)\sin\theta d\theta} \tag{44}$$

With a numerical integration of Eq. (44), we obtain that g_v also approaches the value of 2 asymptotically for very large $\bar{a}_j$ (see SM, J). Hence, the asymptotic value of $g_p = 2$ for very large particles appears to be a general property of RDG scattering for any particle shape. This universal feature may need to be further researched, to develop a full physical explanation. When the dependence of the refractive indices on the wavelength is taken into account, the g_p-limits of 4 at small sizes and 2 at large sizes are slightly different.

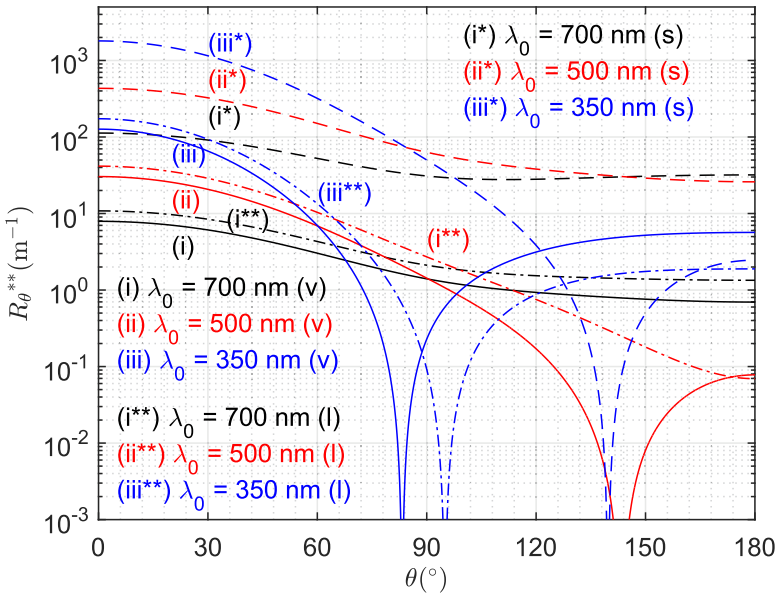

Fig. 3. Specific Rayleigh ratios vs. scattering angles for the RDG regime for dispersions of monodisperse DDAB vesicles (v) with $a_v = 100$ nm, homogeneous spheres (s) with $a = 100$ nm, and liposomes (l) with $a_l = 104.8$ nm for $\lambda_0 = 700$, 500, and 350 nm.

4. Sample calculations

4.1. Conditions and parameters used

The theory for single and independent scattering for the R and RDG regimes introduced in the previous sections is used for describing the scattering properties of vesicles and liposomes for a specific example of DDAB, for which $d_b \approx 2.4$ nm [30] and $d_w \approx 50$ nm (the latter was obtained by extrapolation from Fig. 7 in Ref. [33]). The value of a_c (see Fig. SM1) was assumed to be the same as d_w, for simplicity. The sample calculations were done for a constant medium refractive index $n_m = 1.333$, independent of wavelength, for λ_0 ranging from 350 to 700 nm. Since no data for the refractive index of DDAB were available, a rough estimate of the refractive index $n_s = 1.466$, corresponding to similar surfactant molecules, was used. Then $m_s = 1.10$, and this value was used in the sample calculations here and in Section 5.

4.2. Specific Rayleigh ratios

The specific Rayleigh ratios for homogeneous spheres, vesicles, and liposomes were calculated based on Eq. (31) (see SM, C for detailed expressions). For vesicles, at $\lambda_0 = 700$ nm, the values of R_θ^{**} for $\theta = 0^\circ$ to 180° range from 8 to 0.7 (Fig. 3). These values are much smaller than those for homogeneous spheres by a factor of $0.07 \approx 3d_b/a_v$ (see Eq. (31)). Similar results were obtained for $\lambda_0 = 500$ and 350 nm. For liposomes, for the chosen parameters, the value of a_l closest to 100 nm is 104.8 nm or when $K = 2$. At $\lambda_0 = 700$ nm, the values of R_θ^{**} for $\theta = 0^\circ$ to 180° range from 10 to 1.3 (Fig. 3). Since at $\theta = 0^\circ$ the form factors of a vesicle, a homogeneous sphere, and a liposome are equal to 1, the RDG predictions are the same as the R predictions, and $R_\theta^{**}(0^\circ)$ is proportional to λ_0^{-4}. At $\lambda_0 = 700$ nm, for either vesicles, homogeneous spheres, or liposomes, R_θ^{**} is not zero at any angle. At $\lambda_0 = 500$ nm, R_θ^{**} equals zero at $\theta \approx 143^\circ$ for vesicles only, and there is no zero value for homogeneous spheres or liposomes. At $\lambda_0 = 350$ nm, for homogeneous spheres, R_θ^{**} is zero at $\theta \approx 140^\circ$, for liposomes, R_θ^{**} is zero at $\theta \approx 96^\circ$, and for vesicles at a smaller angle of $\theta \approx 83^\circ$. See SM, K for more calculated results of specific Rayleigh ratios vs. particle radii at various scattering angles.

4.3. Specific turbidities

For RDG specific turbidities for homogeneous spheres, the analytical Eqs. (34) and (35) were used. The results were compared to those obtained by numerical integration of Eq. (33). The results were quite similar, to better than 0.01%, as long as the step size in the numerical integration was sufficiently small ($\leqslant 0.01^\circ$). For τ^{**} for vesicles, the results from the analytical Eqs. (37) and (38) and from the numerical integration, Eq. (33), were also nearly identical. For liposomes, only numerical integration of Eq. (33) and Eq. (39) were used.

For vesicles or liposomes, for $\lambda_0 = 350$ nm to 700 nm, the values of τ^{**} range from 2.1×10^4 to 2.4×10^3 m^{-1} and 3.1×10^4 to 5.3×10^3 m^{-1} with $a_v = 50$ and 100 nm or from 2.2×10^4 to 2.6×10^3 m^{-1} and 4.2×10^4 to 7.8×10^3 m^{-1} with $a_l = 52.4$ and 104.8 nm, respectively (see Fig. 4). For liposomes, the reason for the chosen values of $a_l = 52.4$ nm ($K = 1$) and 104.8 nm ($K = 2$) is the same as described in Section 4.2. These values are much smaller than those of the same-size homogeneous spheres, which range from 2.1×10^5 to 1.9×10^4 m^{-1} and 6.1×10^5 to 1.0×10^5 m^{-1}, respectively. For vesicles of $a_v = 50$ nm, $\tau^{**}(350\,\text{nm}) = 2.1 \times 10^4$ m^{-1} and $\tau^{**}(700\,\text{nm}) = 2.4 \times 10^3$ m^{-1}. The ratio of the specific turbidities is 8.8, different from the R limit of 16 ($\propto \lambda_0^{-4}$) due to the stronger intraparticle interference. In comparison to homogeneous spheres of $a = 50$ nm, $\tau^{**}(350\,\text{nm}) = 2.1 \times 10^5$ m^{-1} and $\tau^{**}(700\,\text{nm}) = 1.9 \times 10^4$ m^{-1}, with a ratio of 11, closer to the R limit of 16. For vesicles, for $\lambda_0 = 700$ nm, τ^{**} is 5.3×10^3 m^{-1} for $a_v = 100$ nm and 2.4×10^3 m^{-1} for $a_v = 50$ nm. The ratio is 2.2, different from 4 ($\propto a_v^2$), with some deviations due to Q_v (see Eq. (37)). For liposomes, for $\lambda_0 = 700$ nm, τ^{**} is 7.8×10^3 m^{-1} for $a_l = 104.8$ nm and 2.6×10^3 m^{-1} for $a_l = 52.4$ nm, with a ratio of 3.0, apart from 8 ($\propto a_l^3$, see Eq. (39)). For comparison, for homogeneous spheres, for $\lambda_0 = 700$ nm, τ^{**} is 1.0×10^5 m^{-1} for $a = 100$ nm and 1.9×10^4 m^{-1} for $a = 50$ nm. The ratio of 5.3 is closer to 8 ($\propto a^3$, see Eq. (34)) with some deviations due to Q_s. See SM, L for more information of specific turbidities of vesicles and liposomes.

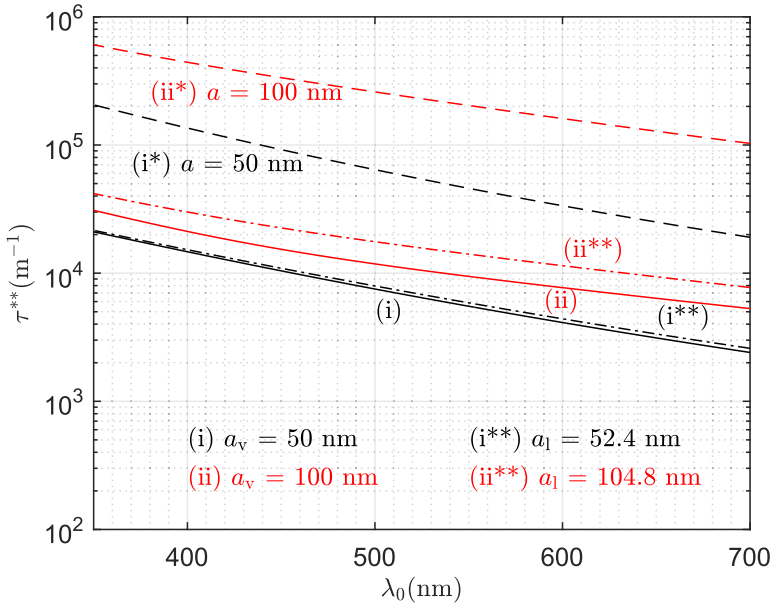

Fig. 4. Specific turbidities vs. wavelengths from 350 to 700 nm for the RDG regime for dispersions of monodisperse vesicles with $a_v = 50$ and 100 nm, homogeneous spheres with $a = 50$ and 100 nm, and liposomes with $a_l = 52.4$ and 104.8 nm.

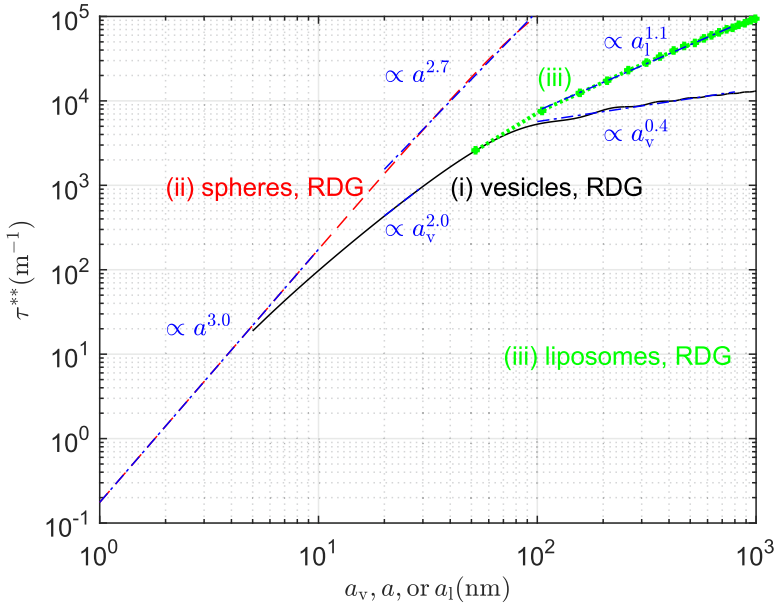

Fig. 5. Specific turbidities vs. particle radii at $\lambda_0 = 700$ nm for the RDG regime for dispersions of monodisperse vesicles, monodisperse homogeneous spheres, and liposomes.

For vesicles, τ^{**} ranges from 1.9×10^1 to 1.3×10^4 m^{-1} for $a_v = 5$ to 1000 nm (see Fig. 5). For $a_v = 20$ to 30 nm, τ^{**} is proportional to ${a_v}^2$, as shown in Eq. (37). For $a_v = 100$ to 800 nm, τ^{**} oscillates slightly with a_v and is proportional to ${a_v}^{0.4}$ because of the use of Q_v, which is smaller than 1 for large vesicles. For homogeneous spheres, τ^{**} ranges from 1.8×10^{-1} to 1.0×10^5 for $a = 1$ to 100 nm. For $a \leqslant 10$, τ^{**} is proportional to $a^{3.0}$, matching the R limit of 3 for small a-value. For $a = 20$ to 100 nm, $\tau^{**} \propto a^{2.7}$, which has a small deviation from the R limit because of the use of $Q_s < 1$ for large homogeneous spheres. For liposomes with $a_l = 52.4$ to 995.6 nm ($K = 1$ to 19 bilayers), at $\lambda_0 = 700$ nm, τ^{**} ranges from 2.6×10^3 to 9.5×10^4 m^{-1} (see Fig. 5). The dependence of τ^{**} on a_v for vesicles is also shown in Fig. 5 for comparison. For vesicles, τ^{**} oscillates slightly with a_v. For liposomes with $a_l = 104.8$ to 786 nm, the average exponent of a_l is 1.1, which is stronger than that of 0.4 for vesicles.

4.4. Wavelength exponents of specific turbidities

The wavelength exponents for homogeneous spheres, vesicles, and liposomes were calculated numerically from Eqs. (42)–(44). Moreover, the exponents for homogeneous spheres and vesicles were also calculated from the analytical Eqs. (42) and (43). The results for those cases were nearly identical, and of course were obtained much more readily.

For vesicles with $a_v = 50$ nm, for $\lambda_0 = 350$ to 700 nm, g_p ranges from 2.6 to 3.6 (see Fig. 6) with some deviations from the R limit of 4. For homogeneous spheres with $a = 50$ nm, for $\lambda_0 = 350$ to

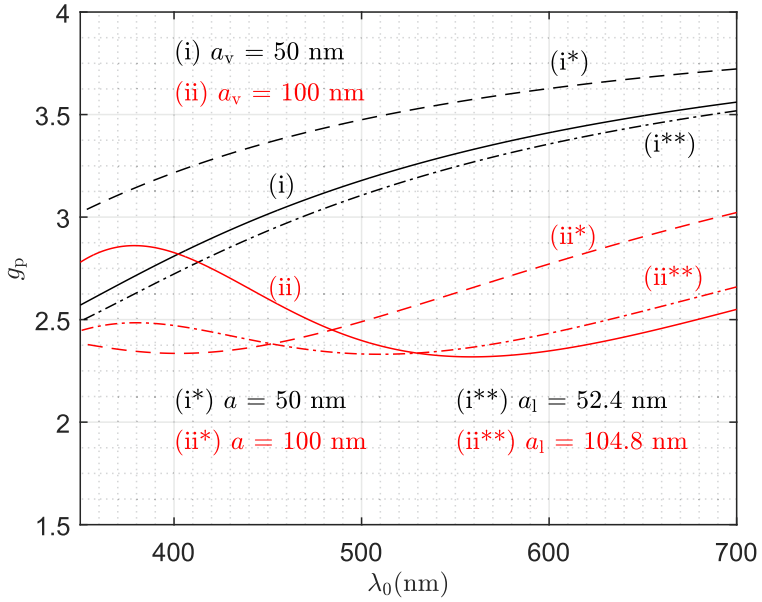

Fig. 6. Wavelength exponents vs. wavelengths from 350 to 700 nm for the RDG regime for dispersions of monodisperse vesicles with $a_v = 50$ and 100 nm, homogeneous spheres with $a = 50$ and 100 nm, and liposomes with $a_l = 52.4$ and 104.8 nm.

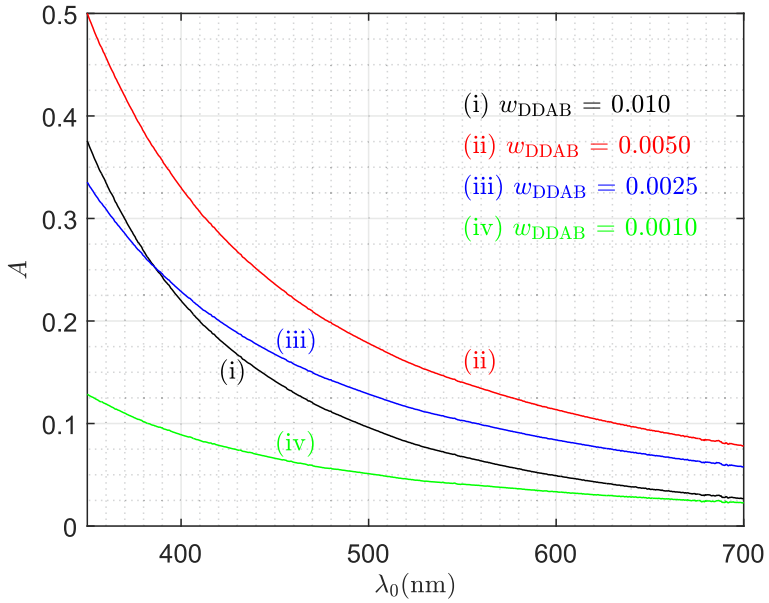

Fig. 7. Absorbance vs. wavelengths from 350 to 700 nm for aqueous dispersions of DDAB vesicles at w_{DDAB} = (i) 0.010, (ii) 0.0050, (iii) 0.0025, and (iv) 0.0010.

700 nm, g_p ranges from 3.0 to 3.7, due to the use of Q_s. For liposomes with $a_l = 52.4$ nm, for $\lambda_0 = 350$ to 700 nm, g_p ranges from 2.5 to 3.5. For vesicles with $a_v = 100$ nm, g_p ranges from 2.3 to 2.9, which oscillates with λ_0 with a minimum at 550 nm and a maximum at 375 nm. For homogeneous spheres with $a = 100$ nm, g_p shows a minimum of 2.3 at 400 nm and a maximum of 3.0 at 700 nm. For liposomes with $a_l = 104.8$ nm, g_p ranges from 2.3 to 2.7, which also oscillates with λ_0 with a minimum at 510 nm and a maximum at 700 nm with a smaller amplitude. See SM, L for more calculated results of wavelength exponents of vesicles and liposomes.

5. Spectroturbidimetry data for DDAB vesicles

Preliminary experimental tests of the equations of τ^{**} for vesicles are presented, as a proof of concept of the equations derived in Sections 3.3. Aqueous dispersions of DDAB vesicles with $w_{DDAB} = 0.010$ (1.0 wt%) were prepared via magnetic stirring, followed by membrane extrusion with a membrane pore size diameter of 400 nm [8]. The aqueous dispersion was further diluted to $w_{DDAB} = 0.0050$, 0.0025, or 0.0010. Absorbance measurements for $\lambda_0 = 350$ to 700 nm were obtained with an Agilent Cary 60 UV–vis spectrometer. Quartz cells with a pathlength of 1 cm were used.

Spectra were obtained three times for each sample, and the results were quite reproducible and then they were averaged (Fig. 7). As w_{DDAB} decreased from 0.010 to 0.0050, all absorbances increased. This is surprising and implies significant effects of multiple scattering, or dependent scattering or both. At $w_{DDAB} = 0.0025$ and 0.0010, A decreased, as would be expected. Moreover, the wavelength dependence of each absorbance spectrum looked quite different.

By using Eqs. (SM.34) to (SM.36), the specific turbidities τ^{**} were calculated (Fig. 8). As w_{DDAB} decreased from 0.010 to

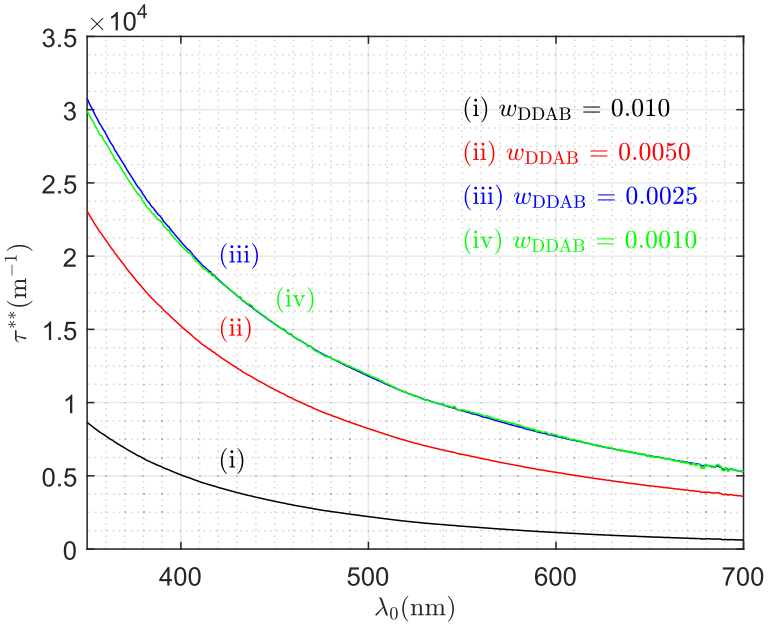

Fig. 8. Specific turbidities vs. wavelengths from 350 to 700 nm for aqueous dispersions of DDAB vesicles at w_{DDAB} = (i) 0.010, (ii) 0.0050, (iii) 0.0025, and (iv) 0.0010.

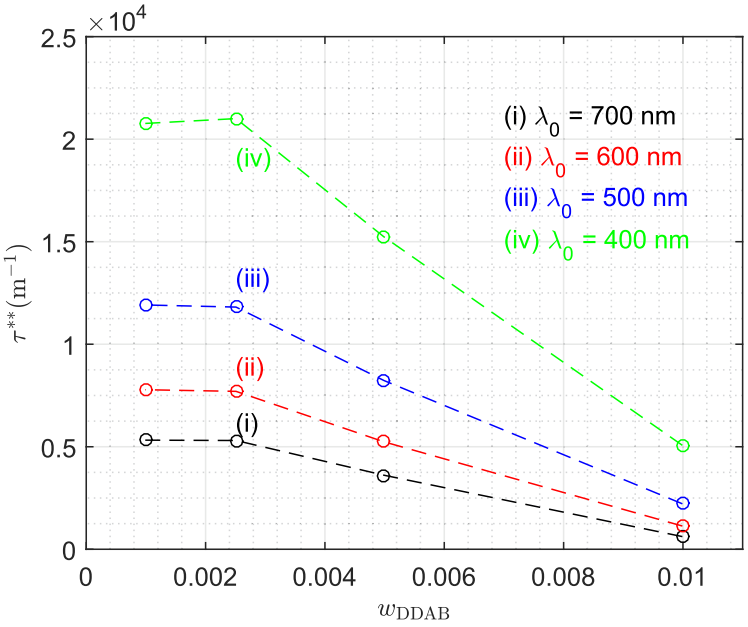

Fig. 9. Specific turbidities vs. weight fractions of DDAB from 0.010 to 0.0010 for aqueous dispersions of DDAB vesicles at λ_0 = (i) 700, (ii) 600, (iii) 500, and (iv) 400 nm.

Table 1
Average radii of DDAB vesicles from specific turbidities for samples at w_{DDAB} = 0.0025 (iii) or 0.0010 (iv) at various wavelengths, for $m_s = 1.10$ and $d_b = 2.4$ nm.

λ_0 (nm)	τ^{**} (m^{-1})		a_v^* (nm)	
	(iii)	(iv)	(iii)	(iv)
700	5300 ± 30	5300 ± 40	100 ± 1	101 ± 1
650	6300 ± 30	6300 ± 200	99 ± 1	99 ± 7
600	7700 ± 20	7800 ± 200	100 ± 1	103 ± 8
550	9400 ± 10	9500 ± 200	100 ± 1	102 ± 5
500	12000 ± 100	12000 ± 300	100 ± 2	102 ± 4
450	15000 ± 100	15000 ± 200	100 ± 1	101 ± 1
400	21000 ± 100	21000 ± 100	99 ± 1	98 ± 1
350	31000 ± 200	30000 ± 300	99 ± 1	96 ± 1

0.0050, τ^{**} increased, again confirming the hypothesis of multiple or dependent scattering due to interparticle interactions, which are not accounted in the equations presented here. For $w_{DDAB} = 0.0025$, τ^{**} increased even more. At 0.0010, it was essentially the same, implying that the limit of single and independent scattering is reached at $w_{DDAB} \leqslant 0.0025$ (see Fig. 9). Some slope fluctuations were also observed, which is most likely due to the small absorbances at the smallest w_{DDAB}.

Hence, these data can be used with the previously derived equations to estimate vesicle sizes without complications due to interparticle effects. The vesicle sizes were determined from the data for $d_b = 2.4$ nm, $n_m = 1.333, n_s = 1.466$ ($m_s = 1.10$). Since the equations apply to monodisperse sizes, average vesicle radii are determined with this approach; see Table 1. The average radii were ca. 100 nm, for all wavelengths considered. This may be due to the actual weak dependence of m_s on wavelength. The DLS radii were also obtained for comparison. They were 107 ± 4 nm at w_{DDAB} = 0.0025 (sample (iii)), and the somewhat different value of 129 ± 5 nm at w_{DDAB} = 0.0010 (sample (iv)). Still the results obtained from ST and DLS were in fair agreement. Since specific turbidities have a weaker dependence on particle sizes, ST is probably less sensitive to the effects of size distribution but more robust than DLS. The sensitivity of the determined average sizes to the values of m_s and d_b used in the estimation of vesicle sizes is examined in SM, M. The results change little when the value of d_b is changed to 2.3 or 2.5 nm (see SM, M). But the estimated sizes change significantly when m_s is changed to 1.09 or 1.11. Hence, for a more accurate determination of average vesicle sizes, one needs to use accurate data of n_m, n_s, and m_s at each wavelength.

6. Conclusions

For a dispersion of vesicles in the R scattering regime, and for single and independent scattering, new analytical solutions have been obtained for (a) the light scattering intensity $i_{s,N}$ and specific Rayleigh ratio R_θ^{**}, and (b) the turbidity τ and specific turbidity τ^{**}. These solutions follow directly from the simple observation that $m_v - 1$, where m_v is the effective relative refractive index, is inversely proportional to the vesicle radius a_v and proportional to the bilayer thickness d_b. These solutions reveal for the first time that $i_{s,N}$ and τ^{**} are proportional to $a_v{}^2 d_b$. This result can be used to determine the particle size of vesicles in the R regime. Similar results for liposomes lead to $m_l - 1$ being proportional to $\left(\frac{d_b}{d_w+d_b}\right)$, and to $i_{s,N}$ and τ^{**} being proportional to $a_l{}^3\left(\frac{d_b}{d_w+d_b}\right)$. These results represent a new advance, not recognized in any relevant references [20–23]. Despite their scientific significance, these results for R scattering are, on their own, of limited practical value, because for wavelengths of 350 to 700 nm, the size limit of applicability of the R regime is quite small, 4 to 10 nm. Most vesicles and all liposomes have larger sizes than the R limit. Nonetheless, the result for R scattering opens the door to solving the problems for $i_{s,N}$ and τ^{**} for the RDG scattering, in which the form factor for vesicles and liposomes have been available for decades. The size limits for the RDG scattering for typical vesicles and liposomes are quite large, because $m_p - 1$ decreases with increasing size for vesicles and is small for liposomes. The limits are about 800 to 2000 nm for liposomes and there is essentially no limit for most vesicles of interest. This had not been known previously [17,21,23,20]. Having for the first time the complete RDG solution for vesicles implies that the light scattering method can be used to determine particle sizes, as demonstrated here experimentally. Previous papers lacked one or more key aspects of the new results. Koch indicated the dependence of the wavelength exponent g_p on particle sizes or shapes but did not report a closed-form analytical expression and did not recognize the explanation of the limiting values of g_p [17]. Chong et al. reported expressions of the scattering intensity and the specific turbidity, but not closed-form expressions of them or any predictions of the limit of the RDG wavelength exponent [21]. van Zanten et al. reported valuable SLS data of relative intensities vs scattering angle for vesicles and used them for determining vesicle sizes. Nonetheless, they did not recognize the dependence of $m_v - 1$ on the vesicle size and did not report data of absolute scattered intensities [22]. Pencer et al. had reported on the effects of vesicle shape, size, and polydispersity on SLS and DLS measurements from simulated light scattering data but did not derive expressions of absolute light scattering intensities as a function of vesicle size [23]. Wang et al. used an extended Lorenz-Mie model for light scattering of vesicles, and calculated turbidities numerically, with no explicit reference to the refractive indices used. They studied the potential errors in the turbidity measurements from scattering at very small angles. They did not report any analytical expressions on the dependence of the effective refractive indices and turbidities on vesicle sizes [20]. In most prior sources, the form factor was used for calculating relative but not absolute intensities, as done here for absolute specific Rayleigh ratios and specific turbidities. The new complete solutions of the R and RDG problems for vesicles and liposomes will allow use by experimental researchers, who may wish to determine sizes and size distributions, with a separate and perhaps easier method than DLS. DLS is easy to use and sensitive and is used routinely in vesicle size characterization. The obtained signal has a very strong size dependence, $a_p{}^n$, with n up to 6 [14]. For this reason, as is well known, a small mass fraction of large vesicles or liposomes can have such a strong contribution to the total signal that the "intensity-average" or "mass-average" size may become inaccurate or even unreliable. As shown here for the first time, the static light scattering methods are less sensitive to size, with n = 2 to 0.4 or 2 to 1. This makes them more robust than DLS for wide size distributions. The new equations may not be directly applicable to non-dilute dispersions for which the specific Rayleigh ratios and the specific turbidities may depend on the surfactant weight fraction w_{surf}. Then interparticle interference occurs, and the structure factors may not be negligible, and have to be modeled separately, in order to be calculated from data. If the goal is to determine vesicle sizes, such dispersions may be diluted to weight fractions sufficiently small that the structure factors are equal to 1. Then the sizes can be determined, as done here for the DDAB example.

Declaration of Competing Interest

The authors declare that they have no known competing financial interests or personal relationships that could have appeared to influence the work reported in this paper.

Acknowledgements

We thank the National Science Foundation (Grant #1706305) for partial support of this research. We also thank Professor Bryan Boudouris and You-Yeon Won, from Purdue University, for the use of the spectrophotometer and the DLS instrument.

Appendix A. Supplementary data

Supplementary data associated with this article can be found, in the online version, at https://doi.org/10.1016/j.jcis.2020.05.085.

References

[1] G. Bozzuto, A. Molinari, Liposomes as nanomedical devices, Int. J. Nanomed. 10 (2015) 975–999, https://doi.org/10.2147/IJN.S68861.

[2] D.M. Patel, R.H. Jani, C.N. Patel, Ufasomes: a vesicular drug delivery, Syst. Rev. Pharm. 2 (2) (2011) 72–78, https://doi.org/10.4103/0975-8453.86290.
[3] R.B. Ashman, B.W. Ninham, Immunosuppressive effects of cationic vesicles, Mol. Immunol. 22 (5) (1985) 609–612, https://doi.org/10.1016/0161-5890(85)90185-3.
[4] P. Schwille, S. Diez, Synthetic biology of minimal systems synthetic biology of minimal systems, Crit. Rev. Biochem. Mol. Biol. 44 (4) (2009) 223–242, https://doi.org/10.1080/10409230903074549.
[5] M. Dubois, T. Gulik-Krzywicki, B. Cabane, Growth of silica polymers in a lamellar mesophase, Langmuir 9 (3) (1993) 673–680, https://doi.org/10.1021/la00027a011.
[6] G. Shi, W. Guo, S.M. Stephenson, R.J. Lee, Efficient intracellular drug and gene delivery using folate receptor-targeted pH-sensitive liposomes composed of cationic/anionic lipid combinations, J. Controlled Release 80 (1–3) (2002) 309–319, https://doi.org/10.1016/S0168-3659(02)00017-2.
[7] K. Tahara, S. Tadokoro, Y. Kawashima, N. Hirashima, Endocytosis-like uptake of surface-modified drug nanocarriers into giant unilamellar vesicles, Langmuir 28 (18) (2012) 7114–7118, https://doi.org/10.1021/la300902z.
[8] S. Šegota, D.U.I. Težak, Spontaneous formation of vesicles, Adv. Colloid Interface Sci. 121 (1–3) (2006) 51–75.https://doi.org/10.1016/j.cis.2006.01.002..
[9] W.D. Pyrz, D.J. Buttrey, Particle size determination using TEM: a discussion of image acquisition and analysis for the novice microscopist, Langmuir 24 (20) (2008) 11350–11360, https://doi.org/10.1021/la801367j.
[10] A. Al-Amoudi, J.J. Chang, A. Leforestier, A. McDowall, L.M. Salamin, L.P. Norlén, K. Richter, N.S. Blanc, D. Studer, J. Dubochet, Cryo-electron microscopy of vitreous sections, EMBO J. 23 (18) (2004) 3583–3588, https://doi.org/10.1038/sj.emboj.7600366.
[11] A. Caria, O. Regev, A. Khan, Surfactant-polymer interactions: phase diagram and fusion of vesicle in the didodecyldimethylammonium bromide-poly (ethylene oxide)-water system, J. Colloid Interface Sci. 200 (1998) 19–30, https://doi.org/10.1006/jcis.1997.5310.
[12] O. Regev, A. Khan, Vesicle lamellar transition events in DDAB-water solution, Trends Colloid Interface Sci. VIII (2007) 298–301, https://doi.org/10.1007/bfb0115187.
[13] P. Hiemenz, R. Rajagopalan, Principles of Colloid and Surface Chemistry, Revised and Expanded, third ed., CRC Press, Boca Raton, 1997, https://doi.org/10.1201/9781315274287.
[14] P.A. Hassan, S. Rana, G. Verma, Making sense of Brownian motion: colloid characterization by dynamic light scattering, Langmuir 31 (1) (2015) 3–12, https://doi.org/10.1021/la501789z.
[15] P.J. Wyatt, Differential light scattering: a physical method for identifying living bacterial cells, Appl. Opt. 7 (10) (1968) 1879, https://doi.org/10.1364/ao.7.001879. URL: http://ao.osa.org/abstract.cfm?URI=ao-7-10-1879.
[16] P. Doty, R.F. Steiner, Light scattering and spectrophotometry of colloidal solutions, J. Chem. Phys. 18 (9) (1950) 1211–1220, https://doi.org/10.1063/1.1747913.
[17] A.L. Koch, Some calculations on the turbidity of mitochondria and bacteria, Biochim. Biophys. Acta 51 (3) (1961) 429–441, https://doi.org/10.1016/0006-3002(61)90599-6. URL: https://www.sciencedirect.com/science/article/pii/0006300261905996.
[18] W. Heller, W.J. Pangonis, Theoretical investigations on the light scattering of colloidal spheres. I. The specific turbidity, J. Chem. Phys. 26(3) (1957) 498–506. https://doi.org/10.1063/1.1743332.
[19] E.I. Franses, L.E. Scriven, W.G. Miller, H.T. Davis, Interpreting the appearance of dispersed systems: I. Model dispersions of polymer latex microspheres, J. Am. Oil Chemists Soc. 60 (5) (1983) 1029–1042, https://doi.org/10.1007/BF02660226.
[20] A. Wang, C. Chan Miller, J.W. Szostak, Core-shell modeling of light scattering by vesicles: effect of size, contents, and lamellarity, Biophys. J. 116 (4) (2019) 659–669.https://doi.org/10.1016/j.bpj.2019.01.006. URL: https://www.sciencedirect.com/science/article/pii/S0006349519300220.
[21] C.S. Chong, K. Colbow, Light scattering and turbidity measurements on lipid vesicles, BBA - Biomembranes 436 (2) (1976) 260–282, https://doi.org/10.1016/0005-2736(76)90192-9. URL: https://www.sciencedirect.com/science/article/pii/0005273676901929.
[22] J.H. van Zanten, H.G. Monbouquette, Phosphatidylcholine vesicle diameter, molecular weight and wall thickness determined by static light scattering, J. Colloid Interface Sci. 165 (2) (1994) 512–518, https://doi.org/10.1006/jcis.1994.1256. URL: https://www.sciencedirect.com/science/article/pii/S0021979784712562.
[23] J. Pencer, F.R. Hallett, Effects of vesicle size and shape on static and dynamic light scattering measurements, Langmuir 19 (18) (2003) 7488–7497, https://doi.org/10.1021/la0345439.
[24] C.F. Bohren, D.R. Huffman, Absorption and Scattering of Light by Small Particles, Wiley, New York, 1983.
[25] M. Kerker, The Scattering of Light, and Other Electromagnetic Radiation, Physical Chemistry, vol. 16, Academic Press, New York, 1969.
[26] H.C. v. d. H.C. Hulst, Light Scattering by Small Particles, Structure of Matter Series, Wiley, New York, 1957.
[27] Y.J. Yang, D.S. Corti, E.I. Franses, Use of close-packed vesicular dispersions to stabilize colloidal particle dispersions against sedimentation, Langmuir 31 (32) (2015) 8802–8808, https://doi.org/10.1021/acs.langmuir.5b02133.
[28] Y.J. Yang, E.I. Franses, D.S. Corti, Effects of light dispersed particles on the stability of dense suspended particles against sedimentation, J. Phys. Chem. B 123 (4) (2019) 922–935, https://doi.org/10.1021/acs.jpcb.8b10172.
[29] R. Skurtveit, J. Sjöblom, J. Bouwstra, G. Gooris, M.H. Selle, Effect of electrolyte on the phase behavior and emulsion stability in the system didodecyldimethylammonium bromide (DDAB)/dodecane/water, J. Colloid Interface Sci. 152 (1) (1992) 205–217, https://doi.org/10.1016/0021-9797(92)90020-M.
[30] T.H. Zemb, D. Gazeau, M. Dubois, T. Gulik-Krzywicki, Crictical behaviour of lyotropic liquid crystals, Epl 21 (7) (1993) 759–766, https://doi.org/10.1209/0295-5075/21/7/008.
[31] E. Feitosa, J. Jansson, B. Lindman, The effect of chain length on the melting temperature and size of dialkyldimethylammonium bromide vesicles, Chem. Phys. Lipids 142 (1–2) (2006) 128–132, https://doi.org/10.1016/j.chemphyslip.2006.02.001. URL: https://www.sciencedirect.com/science/article/pii/S0009308406000193.
[32] S. Jiang, S. Granick, Controlling the geometry (Janus balance) of amphiphilic colloidal particles, Langmuir 24 (6) (2008) 2438–2445, https://doi.org/10.1021/la703274a.
[33] G.A. Ferreira, W. Loh, Structural parameters of lamellar phases formed by the self-assembly of dialkyldimethylammonium bromides in aqueous solution, J. Braz. Chem. Soc. 27 (2) (2016) 392–401, https://doi.org/10.5935/0103-5053.20150297.
[34] J.S. Pedersen, Analysis of small-angle scattering data from colloids and polymer solutions: modeling and least-squares fitting, Adv. Colloid Interface Sci. 70 (1–3) (1997) 171–210, https://doi.org/10.1016/S0001-8686(97)00312-6. URL: https://www.sciencedirect.com/science/article/pii/S0001868697003126.
[35] K.S. Kolbig, I.S. Gradshteyn, I.M. Ryzhik, A. Jeffrey, I. Scripta Technica, Table of Integrals, Series, and Products, seventh ed., Elsevier, Amsterdam, Boston, 2007. https://doi.org/10.2307/2153347.
[36] J.K. Bloomfield, S.H.P. Face, Z. Moss, Indefinite integrals of spherical Bessel functions, arXiv preprint arXiv:1703.06428 (2017).